Binary Gaussian core model: Fluid-fluid phase separation and interfacial properties

A. J. Archer and R. Evans
H. H. Wills Physics Laboratory, University of Bristol, Bristol BS8 1TL, United Kingdom
(Received 16 May 2001; published 17 September 2001)

Using a mean-field equation of state we calculate the density-concentration phase diagrams for a binary mixture of repulsive Gaussian core particles over a range of size ratios. A simple mean-field density functional (DFT) approach, equivalent to the random phase approximation, is used to calculate the surface tension and density profiles of the interface between the demixed fluid phases of the binary mixture. For certain coexisting states oscillations are found in the density profiles on both sides of the interface, i.e., approaching both bulk phases. The form of the oscillations is determined by the asymptotic decay of the bulk total pairwise correlations, and the onset of oscillations in the interfacial density profiles depends on the location of the crossover line (Fisher-Widom line) in the bulk phase diagram where the asymptotic decay changes from monotonic to damped oscillatory. For certain particle size ratios we find another crossover line that separates a region of the phase diagram where the longest-range decay of the pairwise correlations is damped oscillatory from a region where the longest-range decay is damped oscillatory but with a different wavelength. We argue that many of the predictions of the simple DFT approach should remain valid in more refined treatments.

DOI: 10.1103/PhysRevE.64.041501 PACS number(s): 68.05.Cf, 61.20.Gy, 61.25.Hq, 64.60.Fr

I. INTRODUCTION

In recent years increasing attention has been paid to the properties of a particular ''soft-particle'' model of fluids, namely, the Gaussian core model (GCM) in which particles interact via the repulsive pairwise potential $v(r) = \epsilon \exp(-r^2/R^2)$, where $\epsilon > 0$ sets the energy scale and R the range of the potential. The GCM was introduced in the mid-1970s by Stillinger [1]. It regained some popularity because (i) the GCM can yield a negative thermal expansion coefficient in the liquid phase [2] and (ii) a Gaussian serves as a good approximation for the effective interaction between the centers of mass of two polymer chains in an athermal solvent [3–6].

The mathematical properties of the GCM are of special interest [2] and the phase behavior is rather well established [2,6,7]. In the temperature-density (T,ρ) plane there is a region below $k_BT/\epsilon \simeq 0.01$ where increasing ρ leads to freezing into a fcc phase, followed by a fcc-bcc transition, and then melting so that the fluid is stable at high densities. For $\epsilon^* \equiv \beta\epsilon < 100$ where $\beta = (k_BT)^{-1}$, the fluid is stable at *all* densities. Recently Lang *et al.* [7] and Louis *et al.* [8] have studied the fluid region of the phase diagram using Monte Carlo simulations and integral equation theories. What emerges is that for high densities the hypernetted-chain (HNC) approximation provides an excellent account of the Monte Carlo results for the radial distribution function $g(r)$, structure factor $S(q)$, and equation of state. In the limit $\rho R^3 \to \infty$ it is argued that the HNC closure should become exact [7]. Particularly striking is the observation that a very simple closure, the random phase approximation (RPA), which sets the pair direct correlation function $c^{(2)}(r) = -\beta v(r)$, becomes very accurate for very high densities: $\rho R^3 \gtrsim 5$ [7,8]. This implies that the GCM behaves as a ''mean-field fluid'' over a very wide density and temperature range. As the density increases the correlation hole becomes weaker and $g(r) \to 1$, for all separations of the particles. Such behavior is very different from that of fluids with hard cores where short-ranged (packing induced) correlations always persist. For this soft-core model in the limit $\rho R^3 \to \infty$, the mean inter-particle separation $\rho^{-1/3}$ becomes very much less than R and a central particle interacts with a very large number of neighbors—a classic mean-field situation.

Since the RPA is accurate over such a large range of bulk densities it is tempting to argue [7,8] that the simplest mean-field Helmholtz free energy functional

$$\mathcal{F}[\rho] = \mathcal{F}_{id}[\rho] + \frac{1}{2}\int d\mathbf{r}_1 \int d\mathbf{r}_2 \rho(\mathbf{r}_1)\rho(\mathbf{r}_1)v(|\mathbf{r}_1 - \mathbf{r}_2|) \tag{1}$$

should yield a realistic description of the *inhomogeneous* GCM provided the one-body density $\rho(\mathbf{r})$ does not acquire very small values. The density functional (1) *generates* the RPA: $c^{(2)}(r) = -\beta v(r)$. Physically one is arguing that the excess (over the ideal gas $\mathcal{F}_{id}$) free energy of the fluid can be approximated by the internal energy with the pairwise distribution function $\rho^{(2)}(\mathbf{r}_1,\mathbf{r}_2)$ replaced by its uncorrelated limit $\rho(\mathbf{r}_1)\rho(\mathbf{r}_1)$. Louis *et al.* used the functional (1) to investigate the density profiles of Gaussian core particles adsorbed at a hard wall. Their results agree closely with those from Monte Carlo simulations for $\epsilon^* = 2$ and the three bulk densities $\rho R^3 = 1, 0.5, 0.1$, confirming that the GCM does behave as a mean-field fluid—at least for this type of inhomogeneity [8].

Given the success of the simple mean-field theory in describing the pure fluid it is natural to ask what the corresponding theory yields for a binary mixture of repulsive Gaussian core particles. This question was addressed partially in Ref. [8] and the authors showed that for certain choices of the energy and range parameters fluid-fluid demixing is predicted by the mean-field (RPA) approach. Although it is not clear that this phase separation mimics that which is found in polymer blends [8], the observation that a system with purely repulsive interparticle potentials can separate into two fluid phases is of intrinsic interest. Recall that the pure GCM exhibits only a single fluid phase.

In the present paper we investigate the nature of the interface between the two coexisting fluid phases in the binary GCM using the two-component generalization of Eq. (1), i.e., the density functional that generates the RPA for the three partial pair direct correlation functions $c_{ij}^{(2)}(r)$ of the mixture. We find that in spite of its simplicity this mean-field theory predicts surprisingly structured density profiles; there is a wide range of thermodynamic states where the profiles of both species exhibit oscillations decaying into the bulk on each side of the interface. The occurrence of oscillations is directly related to the form of the asymptotic decay of the total pairwise correlations $h_{ij}(r)$ in the bulk mixture.

Our paper is arranged as follows. In Sec. II we describe the binary GCM and the determination of the bulk binodal (fluid-fluid coexistence curve) within the mean-field approximation, showing how the phase separation varies with the size ratio R_{22}/R_{11}. Section III presents results for the density profiles $\rho_i(z)$, $i=1,2$, and surface tension at the planar fluid-fluid interface. In Sec. IV we determine the asymptotic decay of $h_{ij}(r)$ and the crossover line (Fisher-Widom line) in the bulk phase diagram where the character of the longest-range decay changes from monotonic to oscillatory. The location of these lines determines whether or not oscillations can occur in the interfacial density profiles [9]. For certain size ratios we find a different line, away from the binodal, that separates a region where pairwise correlations exhibit oscillatory decay from a region where the oscillations have a different wavelength. We conclude in Sec. V with a discussion of our results and possible limitations of the mean-field approach for interfacial properties.

II. THE MODEL MIXTURE AND ITS PHASE DIAGRAM

The GCM binary mixture is specified by the pair potentials between particle species i and j. These are given by the Gaussian form

$$v_{ij}(r)=\epsilon_{ij}\exp(-r^2/R_{ij}^2) \tag{2}$$

where $\epsilon_{ij}>0$ denotes the energy and R_{ij} determines the range of the ij interaction; $1\leqslant i,j\leqslant 2$. Thinking of the particles as representing polymers, R_{ii} is roughly the radius of gyration of species i.

We use a simple mean-field form for the intrinsic Helmholtz free energy functional of the inhomogeneous mixture:

$$\mathcal{F}[\{\rho_i\}]=\mathcal{F}_{id}[\{\rho_i\}]+\frac{1}{2}\sum_{ij}\int d\mathbf{r}_1 \times\int d\mathbf{r}_2\rho_i(\mathbf{r}_1)\rho_j(\mathbf{r}_2)v_{ij}(|\mathbf{r}_1-\mathbf{r}_2|) \tag{3}$$

where $\mathcal{F}_{id}$ is the ideal gas part of the free energy functional. Equation (3) is a straightforward generalization to mixtures of the functional introduced in Eq. (1). Recalling that the two-body direct correlation functions are given by

$$c_{ij}^{(2)}(\mathbf{r}_1,\mathbf{r}_2)=-\frac{\beta\delta^2(\mathcal{F}[\{\rho_i\}]-\mathcal{F}_{id}[\{\rho_i\}])}{\delta\rho_i(\mathbf{r}_1)\delta\rho_j(\mathbf{r}_2)}, \tag{4}$$

it follows that

$$c_{ij}^{(2)}(\mathbf{r}_1,\mathbf{r}_2)=c_{ij}^{(2)}(|\mathbf{r}_1-\mathbf{r}_2|)=-\beta v_{ij}(|\mathbf{r}_1-\mathbf{r}_2|), \tag{5}$$

which is the standard random phase approximation. In the bulk mixture the densities are constants, $\rho_i(\mathbf{r})=\rho_i^b$. Writing these in terms of the total density ρ and a composition variable x, such that $\rho_1^b=(1-x)\rho$ and $\rho_2^b=x\rho$, we can write the bulk Helmholtz free energy per particle f as [8]

$$f(\rho,x)=f_{id}(\rho,x)+\frac{1}{2}\rho\hat{V}_0(x). \tag{6}$$

βf_{id} contains the ideal free energy of mixing $x\ln(x)+(1-x)\ln(1-x)$ as well as an irrelevant ρ dependent term. The mean-field interaction term is

$$\hat{V}_0(x)=(1-x)^2\hat{v}_{11}(0)+2x(1-x)\hat{v}_{12}(0)+x^2\hat{v}_{22}(0) \tag{7}$$

where $\hat{v}_{ij}(0)$ is the $\mathbf{q}=0$ limit of the Fourier transform (FT) of the pair potential (the caret denotes a FT with respect to the wave vector $\mathbf{q}$):

$$\hat{v}_{ij}(0)=\int d\mathbf{r}v_{ij}(\mathbf{r})=\pi^{3/2}\epsilon_{ij}R_{ij}^3. \tag{8}$$

Since the free energy (6) has the simple mean-field form, the thermodynamic stability conditions for the binary mixture also take a very simple form and Louis *et al.* [8] showed that fluid-fluid phase separation is possible at constant volume provided

$$\beta^{-1}\chi\equiv 2\hat{v}_{12}(0)-[\hat{v}_{11}(0)+\hat{v}_{22}(0)]>0 \tag{9}$$

or at constant pressure provided

$$\beta^{-2}\Delta\equiv[\hat{v}_{12}(0)]^2-\hat{v}_{11}(0)\hat{v}_{22}(0)>0. \tag{10}$$

In order to observe phase separation we must choose the parameters ϵ_{ij} and R_{ij} so that these conditions are satisfied. The choice of parameters can be restricted further by making contact with simulation studies of binary solutions of self-avoiding polymer coils at infinite dilution [4] in which it was suggested that the effective potentials between the polymer centers of mass could be modeled quite well by the GCM, defined by Eq. (2), with

$$\epsilon_{12}\leqslant\epsilon_{11}=\epsilon_{22} \tag{11}$$

and

$$R_{12}^2=\frac{1}{2}(R_{11}^2+R_{22}^2). \tag{12}$$

Clearly, relation (11) favors mixing; the energy penalty is lower if unlike species are neighbors. It is relation (12) that favors demixing since it implies $R_{12}>(R_{11}+R_{22})/2$, which corresponds to positive nonadditivity, known to drive demixing in hard-sphere mixtures [8]. The majority of our calculations for interfacial properties will be for a mixture with

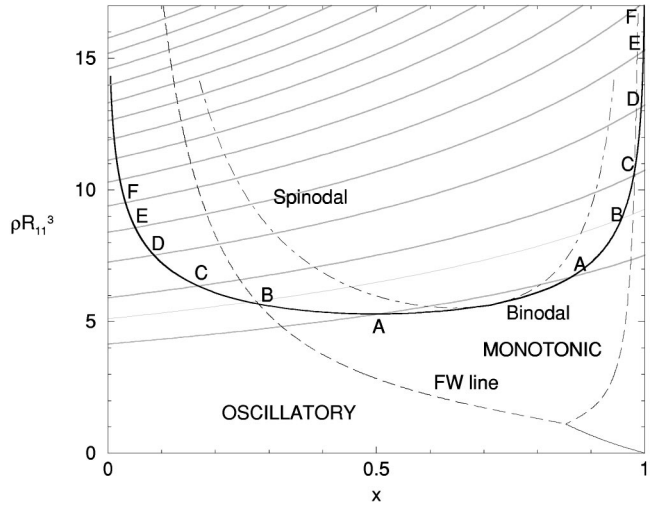

FIG. 1. The bulk phase diagram for a mixture of Gaussian particles with $\epsilon_{12}/\epsilon_{11}=0.944$ and $R_{22}/R_{11}=0.665$, which is equivalent to a mixture of two polymers with length ratio 2:1. ρ is the total density and x is the concentration of the smaller species 2. The gray lines are lines of constant pressure; the lowest is at reduced pressure $P\beta R_{11}^3=100$, the next at $P\beta R_{11}^3=150$, then 200, and the subsequent ones increase in increments of 100. The points marked A–F are the points where the gray lines intersect the binodal (solid line). The density profiles for the corresponding fluid-fluid interfaces are shown in Figs. 6 and 7 below. The dashed line denotes the Fisher-Widom (FW) line where the asymptotic decay of the bulk pairwise correlation functions crosses over from oscillatory to monotonic. The solid line in the bottom right corner denotes a line of crossover from asymptotic oscillatory decay with a certain wavelength to a similar oscillatory decay but with a different wavelength—see Sec. IV.

$\beta\epsilon_{11}\equiv\epsilon_{11}^*=\epsilon_{22}^*=2$, $\epsilon_{12}^*=1.888$, $R_{22}/R_{11}=0.665$, and R_{12} given by Eq. (12). (Henceforward we use R_{11}, the radius of gyration of the longer polymer, as the length scale in our analysis.) This choice of parameters was motivated by the study of Louis *et al.* [8] where the R_{ij} were chosen to model a mixture of self-avoiding polymers with $L=200$ (species 1) and $L=100$ (species 2) monomers. The radius of gyration $R_g\sim L^\nu$ where $\nu\simeq 0.588$ is the Flory exponent.

For $\epsilon^*=2$ the pure GCM remains fluid for all densities. If the mixture is treated within the present mean-field approximation the temperature scales out of the free energy in Eq. (6) and the phase behavior is that of an athermal system [8], depending only on the ratios $\epsilon_{12}/\epsilon_{11}$ and R_{22}/R_{11}. We chose $\epsilon_{12}/\epsilon_{11}$ so that the critical point of the fluid-fluid demixing was the same as that in the mixture considered in Ref. [8], i.e., at $x_c=0.70$, $\rho_c R_{11}^3=5.6$. In Fig. 1 we plot the phase diagram for this particular choice of parameters. The spinodal (dash-dotted line) is obtained as described in Ref. [8]. We determined the binodal by standard procedures. For two demixed phases A and B to be in equilibrium the chemical potentials μ_i and the pressures P of the two phases must be equal, i.e., $\mu_{i,A}=\mu_{i,B}$ for $i=1,2$ and $P_A=P_B$. In terms of $v=1/\rho$, the volume per particle, these quantities are given by

$$\mu_1=f-v\left(\frac{\partial f}{\partial v}\right)_x-x\left(\frac{\partial f}{\partial x}\right)_v, \tag{13}$$

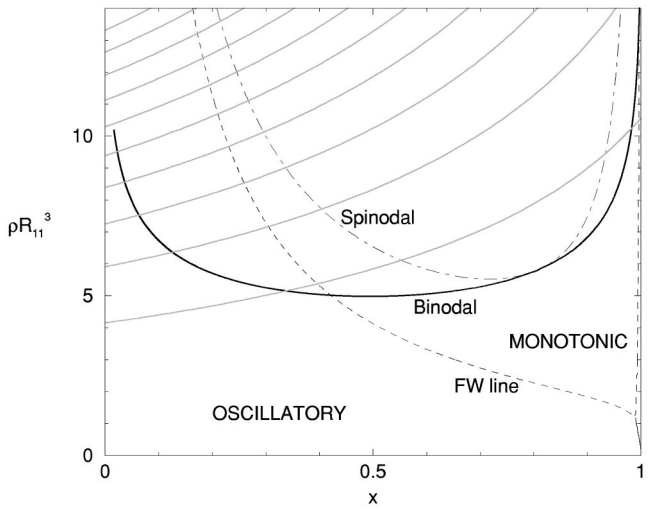

FIG. 2. As in Fig. 1 but now $\epsilon_{12}/\epsilon_{11}=0.825$ and $R_{22}/R_{11}=0.524$, which is equivalent to a mixture of two polymers with length ratio 3:1. The gray lines are lines of constant pressure; the lowest is at reduced pressure $P\beta R_{11}^3=100$ and the others increase in increments of 100. The right hand branch of the FW line (dashed line) lies close to the $x=1$ axis but the solid line in the bottom right corner denoting oscillatory-oscillatory crossover is still present for these parameters.

$$\mu_2=f-v\left(\frac{\partial f}{\partial v}\right)_x+(1-x)\left(\frac{\partial f}{\partial x}\right)_v, \tag{14}$$

and

$$P=-\left(\frac{\partial f}{\partial v}\right)_x. \tag{15}$$

The calculation of the binodal is simpler to perform in the ensemble where the pressure is the independent variable instead of the total density $\rho=1/v$. We Legendre transform to $g=f+Pv$ where $g(x,P)$ is the Gibbs free energy per particle. In this ensemble the conditions of equal chemical potential and pressure lead to the common tangent construction on g:

$$\left(\frac{\partial g}{\partial x}\right)_P\Big|_{x_A}=\left(\frac{\partial g}{\partial x}\right)_P\Big|_{x_B}=\frac{g(x_A,P)-g(x_B,P)}{x_A-x_B} \tag{16}$$

where x_A and x_B are the concentrations of species 2 in phases A and B, respectively.

The gray lines in Fig. 1 denote lines of constant pressure in the (ρ,x) phase diagram. Also plotted is the Fisher-Widom (FW) line to which we shall return later. Other representative phase diagrams are shown in Figs. 2–4. These are obtained from the same mean-field free energy but correspond to different choices of R_{22}/R_{11}, i.e., different length ratios. In each case $\epsilon_{12}/\epsilon_{11}$ is chosen to keep the (total) critical density at a similar value to that of the original mixture. As R_{22}/R_{11} is reduced the critical concentration x_c shifts to higher values and the shape of the FW line is altered significantly.

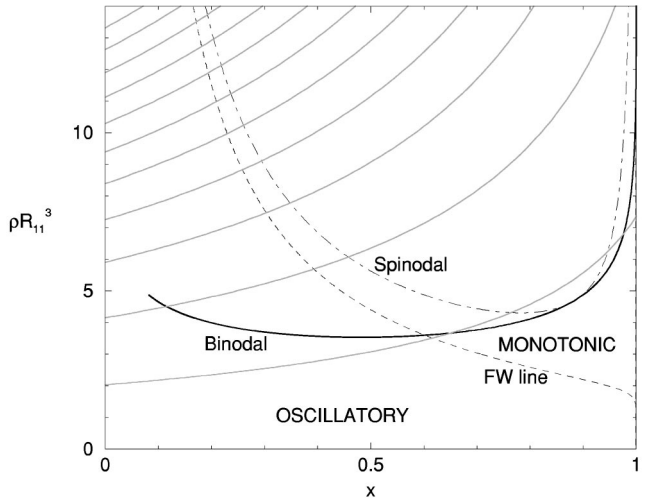

FIG. 3. As in Fig. 1 but now $\epsilon_{12}/\epsilon_{11}=0.70$ and $R_{22}/R_{11}=0.388$, which is equivalent to a mixture of two polymers with length ratio 5:1. The gray lines are lines of constant pressure; the lowest is at reduced pressure $P\beta R_{11}^3=25$, the next at $P\beta R_{11}^3=100$, and then increasing in increments of 100. It becomes increasingly difficult to determine the binodal as P is increased; the coexisting phase to the right is almost pure species 2 ($x=1$) and the total density ρ becomes very high. The right hand branch of the FW line and the oscillatory-oscillatory crossover cannot be seen due to their proximity to the $x=1$ axis.

Finally in Fig. 5 we consider a different class of mixture described by the parameters $\epsilon_{11}^*=\epsilon_{22}^*=2$, $\epsilon_{12}^*=2.07$, and $R_{11}=R_{22}=R_{12}$. Now the demixing occurs not because of the nonaddivity of the R_{ij} but because there is a lower energy penalty when like species are neighbors. The phase diagram is symmetrical about $x=0.5$. We shall find that several of the interfacial properties are quite different in this class of mixture from those in the former class.

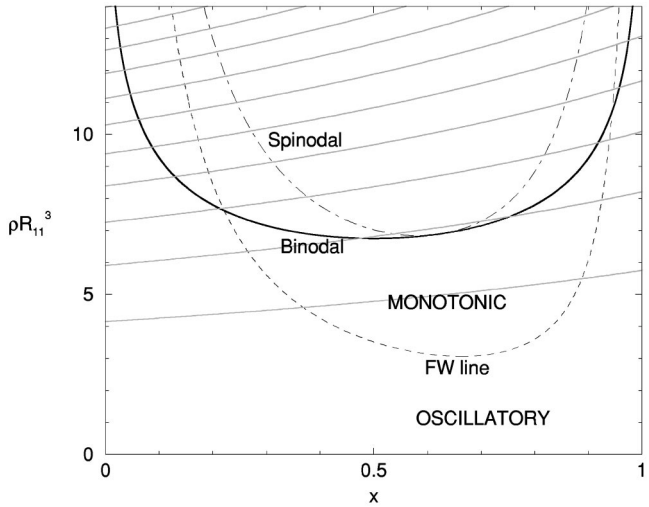

FIG. 4. As in Fig. 1 but now $\epsilon_{12}/\epsilon_{11}=1.0$ and $R_{22}/R_{11}=0.8$, which is equivalent to a mixture of two polymers with length ratio 1.46:1. The gray lines are lines of constant pressure; the lowest is at reduced pressure $P\beta R_{11}^3=100$ and the others increase in increments of 100. For these parameters there is no crossover line between two types of oscillatory decay and no cusp in the FW line.

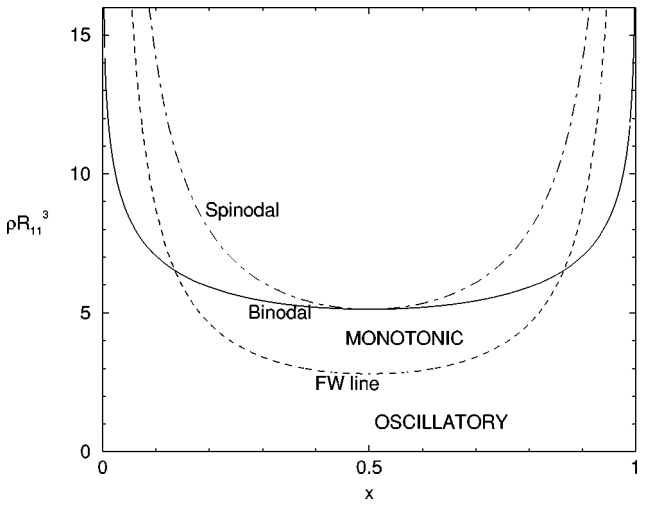

FIG. 5. As in Fig. 1 but now $\epsilon_{12}/\epsilon_{11}=1.035$ and $R_{22}/R_{11}=1.0$. In this symmetrical case there is no crossover line between two types of oscillatory decay and no cusp in the FW line. Note the perfect symmetry about the line $x=0.5$. The tie lines are horizontal in this case.

III. PROPERTIES OF THE FLUID-FLUID INTERFACE

In this section we investigate the one-body density profiles $\rho_i(z)$, $i=1,2$, and the surface tension γ for the planar interfaces that arise between coexisting fluid phases in the GCM. Since our approach is based on the mean-field free energy functional (3) effects of capillary-wave fluctuations are omitted and (away from the critical point) the interfacial width remains finite in vanishing gravitational field. Thus we work with the grand potential functional

$$\Omega_V[\{\rho_i\}]=\mathcal{F}[\{\rho_i\}]-\sum_i \int d\mathbf{r}[\mu_i-V_i(\mathbf{r})]\rho_i(\mathbf{r}), \quad (17)$$

taking from the outset the external potentials $V_i(\mathbf{r})=V_i(z)=0$, $i=1,2$. This procedure yields well-defined planar density profiles $\rho_i(z)$, with z normal to the surface, from which the surface tension can be calculated.

A. Density profiles

In order to calculate the equilibrium density profiles across the free interface we take the functional derivative of Eq. (17) which, using Eq. (3) and in the absence of an external field, yields the Euler-Lagrange equation

$$\mu_i=\mu_{i,id}(\rho_i(z_1))+\sum_j \int d\mathbf{r}_2\rho_j(z_2)v_{ij}(|\mathbf{r}_1-\mathbf{r}_2|). \quad (18)$$

$\mu_{i,id}$ is the chemical potential of species i in an ideal gas and $\beta\mu_{i,id}(\rho_i)=\ln(\Lambda_i^3\rho_i)$ (Λ_i is the thermal de Broglie wave-

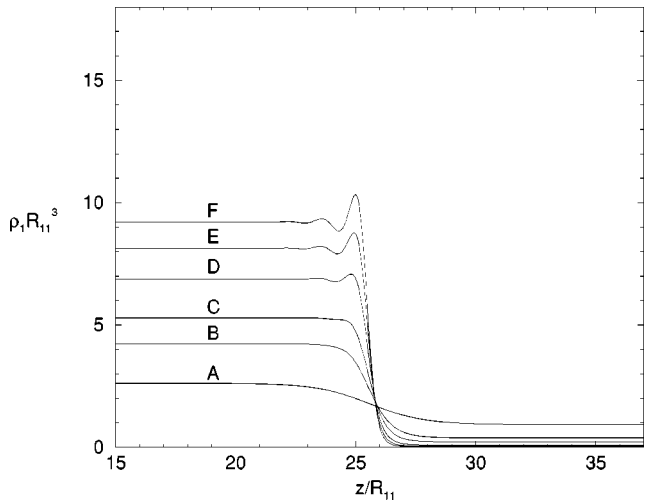

FIG. 6. The equilibrium density profiles of species 1, the larger particles, at the planar interface between coexisting fluid phases for states specified in Fig. 1, i.e., a mixture of two polymers with length ratio 2:1. For state *A* near the critical point, the interface is broad, whereas far from the critical point, states *E* and *F*, the interface becomes much sharper. Oscillatory profiles are found for states *C*–*F*.

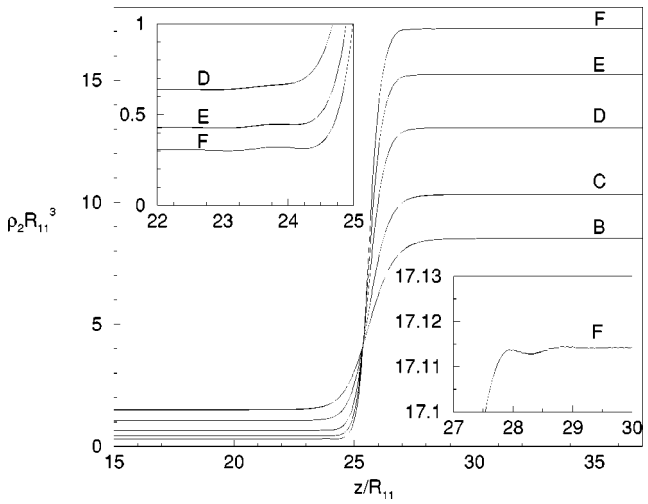

FIG. 7. The equilibrium density profiles of species 2, the smaller particles, corresponding to Fig. 6. The insets show magnifications of regions where the profiles exhibit oscillations. Note that the profiles of both species decay into a given bulk state with the same decay length and, when oscillatory, the same wavelength. The amplitude and the phase do depend on the species.

length). Eliminating the chemical potentials in favor of the bulk coexisting densities ρ_i^b that were found from the calculation of the binodal, we have

$$\rho_i(z_1)=\rho_i^b \exp\left[\sum_j \int d\mathbf{r}_2[\rho_j^b-\rho_j(z_2)]v_{ij}(|\mathbf{r}_1-\mathbf{r}_2|)\right]. \quad (19)$$

This coupled pair of equations can be solved self-consistently for the density profiles of the two species. The results for a mixture of Gaussian particles representing a mixture of polymers of length ratio 2:1 are shown in Figs. 6 and 7. The striking feature is the development of pronounced oscillations in the density profile of the larger species, $\rho_1(z)$, for states well removed from the critical point. Closer inspection shows that for states *C*, *D*, *E*, and *F both* density profiles $\rho_1(z)$ and $\rho_2(z)$ exhibit nonmonotonic decay into the bulk phase that is rich in species 1. On the other side of the interface, approaching the bulk phase rich in species 2, magnification shows that both $\rho_1(z)$ and $\rho_2(z)$ are nonmonotonic for states *D*, *E*, and *F*. For states *A* and *B*, closer to the critical point, there is no sign of oscillations on either side of the interface.

This is not the first time that damped oscillatory density profiles have been calculated for fluid-fluid interfaces treated by DFT. Evans *et al.* [9] found that the planar liquid-vapor density profiles for a one-component square-well fluid treated by means of a nonlocal weighted density approximation for repulsive forces exhibited oscillations on the liquid side of the interface provided the thermodynamic state lay sufficiently far from the bulk critical point. The oscillations we find for species 1 in the present calculations are considerably more pronounced than those found in Ref. [9] and resemble those found for the colloidal profile in a recent DFT study [10] of a model colloid–(ideal) polymer mixture in which colloid-colloid and colloid-polymer interactions are hard-sphere-like. The oscillations were found in both the colloid and polymer profiles but only on the colloid rich side of the interface. Here we find, for a range of thermodynamic states, oscillations on *both* sides of the interface. Moreover, these oscillations arise for a system in which the interparticle potentials are very soft and are treated by means of the simplest mean-field DFT.

In the original analysis of oscillatory one-body density profiles $\rho(z)$ at the liquid-vapor interface it was shown [9] that oscillations should occur when the bulk fluid, in that case a liquid, lies on the oscillatory side of the FW line. The latter divides the bulk phase diagram into regions where the longest-range decay of $rh(r)$ is either pure exponential or (exponentially) damped oscillatory [11]. $h(r)=g(r)-1$ is the total pairwise correlation function of the fluid. It was also argued that the wavelength and the decay length of the oscillations in $\rho(z)$ as $z\to\infty$ (deep into the bulk phase) should be identical to those characterizing the asymptotic decay ($r\to\infty$) of $rh(r)$ [9]. In order to understand the genesis of oscillations in $\rho_1(z)$ and $\rho_2(z)$ for our present model we calculated the FW line for the bulk mixture, now defined as the line in the phase diagram where the leading asymptotic decay of all three pairwise correlation functions $h_{ij}(r)$, $1\leqslant i,j\leqslant 2$, crosses over from monotonic to oscillatory; these FW lines are shown in Figs. 1–5. Details of the calculations are described in Sec. IV. Here it suffices to say that we find oscillations on both sides of the interface when the tie lines intersect both sides of the binodal at points that lie above the two intersections of the FW line (this has two branches) with the binodal, i.e., states *D*, *E*, and *F* in Fig. 1. A similar situation occurs for the more symmetrical case $\epsilon_{12}/\epsilon_{11}=1.0$ and $R_{22}/R_{11}=0.8$, shown in Fig. 4. However, for the more asymmetrical cases in Figs. 2 and 3 where the right hand branch of the FW line lies very close to the $x=1$ axis and therefore

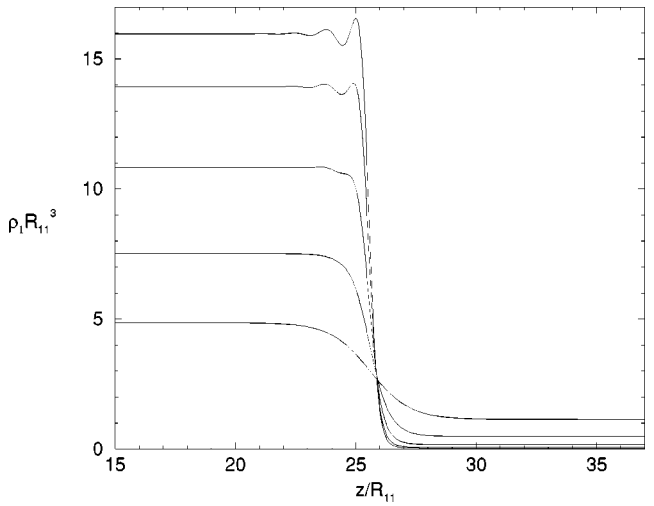

FIG. 8. Equilibrium density profiles of species 1 for the symmetric mixture with $\epsilon_{12}/\epsilon_{11}=1.035$ and $R_{22}/R_{11}=1.0$ whose phase diagram is given in Fig. 5. The density profiles are calculated at total bulk densities $\rho R_{11}^3=6$, 8, 11, 14, and 16 (from bottom to top in the left hand phase). The density profiles of species 2 are merely reflections of these profiles in the line $z/R_{11}=25.6$.

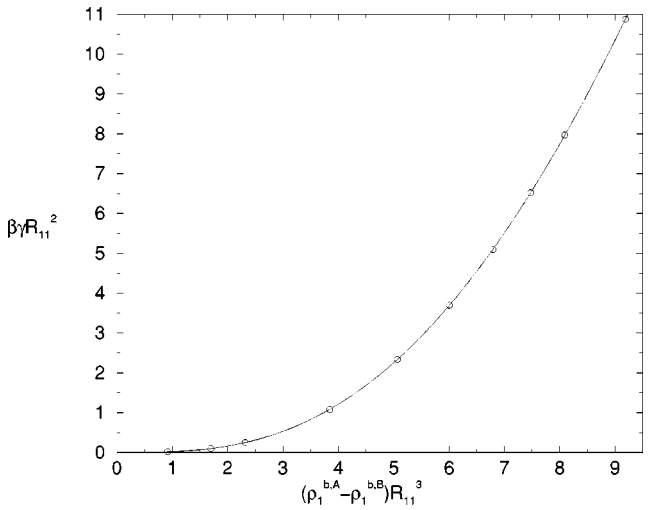

FIG. 9. The reduced surface tension $\gamma^*=\beta\gamma R_{11}^2$ calculated for the planar interface between coexisting fluid phases in the system specified in Fig. 1, i.e., a mixture of two polymers with length ratio 2:1. $(\rho_1^{b,A}-\rho_1^{b,B})R_{11}^3$, the difference in density of species 1 between bulk phases A and B, and γ vanish at the critical point. The circles are the results of our calculations and the solid line joining these is a guide to the eye.

intersects the binodal at very high densities, oscillations are observable at fairly low pressures on the side of the interface rich in species 1 (small x) whereas for the side rich in species 2 very high pressures are required before the oscillations arise.

For the perfectly symmetrical mixture $R_{22}/R_{11}=1.0$, whose phase diagram is shown in Fig. 5, the binodal and the FW line are symmetric about $x=0.5$ and the density profiles $\rho_1(z)$ and $\rho_2(z)$ are simply reflections of each other—see Fig. 8. Because of the symmetry, if oscillations occur in the profiles on one side of the interface they must occur on the other side. As can be seen from Fig. 5, the intersection of the FW line with the binodal is at a total density not very far above the critical density and oscillatory profiles should occur for $\rho R_{11}^3>6.5$. However, for states not too far above the intersection of the FW line and the binodal the amplitude of the oscillatory contribution to the profile is often small, making it difficult to distinguish this contribution in the numerical results.

The general theory of the asymptotic decay of correlations in fluid mixtures with short-ranged interparticle potentials predicts [12] that the longest-range decay of the profiles should be

$$\rho_i(z)-\rho_i^b \sim \rho_i^b A_i \exp(-\alpha_0 z), \quad z\to\infty, \tag{20}$$

on the monotonic side of the FW line and

$$\rho_i(z)-\rho_i^b \sim \rho_i^b \tilde{A}_i \exp(-\tilde{\alpha}_0 z)\cos(\alpha_1 z-\theta_i), \quad z\to\infty, \tag{21}$$

on the oscillatory side. Equivalent relations apply for $z\to-\infty$, with the appropriate identification of the bulk densities ρ_i^b. The decay lengths α_0^{-1} and $\tilde{\alpha}_0^{-1}$ and the wavelength of oscillations $2\pi/\alpha_1$ are properties of the bulk fluid and are the same for both species (see Sec. IV). Only the amplitudes A_i and $\tilde{A}_i$ and, for oscillatory profiles, the phase θ_i depend on the particular species i. Our numerical results are consistent with these general predictions. Note that on the FW line $\alpha_0=\tilde{\alpha}_0$ and that for states near this line both types of contribution must be taken into account.

B. Surface tension

Having calculated the equilibrium density profiles at the free interface, these can be used to obtain the surface tension of the interface. The latter is defined as the excess grand potential per unit area and can be written as

$$\gamma=\int_{-\infty}^{\infty} dz[P+\omega(z)] \tag{22}$$

where P is the bulk pressure at coexistence and $\omega(z)$ is the grand potential density obtained from Eqs. (3) and (17) with $V_i(z)=0$. The reduced tension $\gamma^*=\beta\gamma R_{11}^2$ is plotted in Fig. 9 for the interfaces corresponding to Figs. 6 and 7, i.e., the phase diagram of Fig. 1. We have chosen to plot γ^* versus the order parameter $(\rho_1^{b,A}-\rho_1^{b,B})R_{11}^3$, where $\rho_1^{b,A}$ is the bulk density of species 1 in phase A, rich in species 1, and $\rho_1^{b,B}$ is the same quantity in phase B, poor in species 1 [13]. On approaching the critical point simple mean-field arguments imply that γ^* should vanish as $(\rho_1^{b,A}-\rho_1^{b,B})^3$ and this is confirmed by our numerical results. A similar plot of γ^* for the perfectly symmetric mixture is displayed in Fig. 10. Note that for a given value of $(\rho_1^{b,A}-\rho_1^{b,B})R_{11}^3$, γ^* is significantly larger for the asymmetric mixture (Fig. 9).

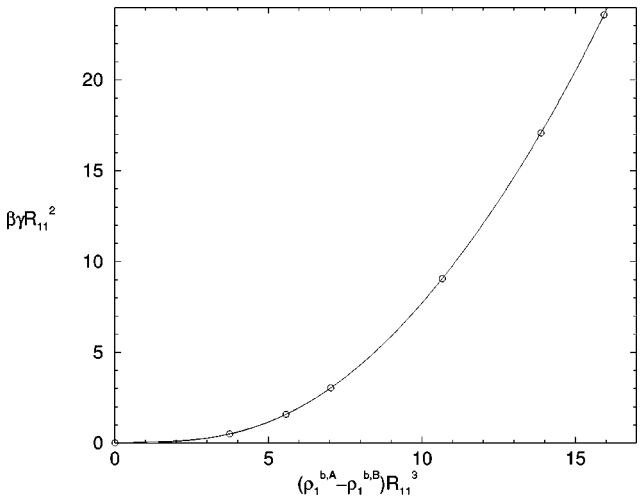

FIG. 10. The reduced surface tension $\gamma^* = \beta\gamma R_{11}^2$ calculated for the planar interface between coexisting fluid phases in the perfectly symmetric system specified in Fig. 5. $(\rho_1^{b,A} - \rho_1^{b,B})R_{11}^3$, the difference in density of species 1 between bulk phases A and B, and γ vanish at the critical point. The circles are the results of our calculations and the solid line joining these is a guide to the eye.

We can obtain an estimate for the surface tension of a phase separated mixture of ''polymers'' by choosing $\gamma^* = 5$, corresponding to a state well removed from the critical point, $T = 300$ K and $R_{11} = 20$ nm. We find $\gamma = 52$ μN/m, a value one order of magnitude greater than that calculated and measured for a colloid-polymer mixture [13], but two orders of magnitude smaller than the tensions of simple atomic fluids near their triple points.

Further insight into the factors that determine the surface tension in our binary mixtures can be obtained by working with linear combinations of the density profiles $\rho_1(z)$ and $\rho_2(z)$. The total number density $N(z)$ and a local concentration variable $C(z)$, the surface segregation, may be defined for a fluid-fluid interface by

$$N(z) = \rho_1(z) + \rho_2(z), \tag{23}$$

$$C(z) = \frac{x\rho_1(z) - (1-x)\rho_2(z)}{x(1-x)}, \tag{24}$$

where x is the concentration of species 2 in the bulk liquid phase. These variables are normally introduced for a liquid-gas interface. For the situation where the ''gas'' phase has a nonzero density, the integral over $C(z)$ diverges. When the densities of both phases are comparable, $C(z)$ should be replaced by the symmetrized segregation [14]

$$\Delta(z) = \frac{a_2[\rho_1(z) - \rho_1^{b,A}] - a_1[\rho_2(z) - \rho_2^{b,A}]}{a_1 a_2} \tag{25}$$

where the a_i are given by

$$a_i = \frac{\rho_i^{b,A} - \rho_i^{b,B}}{(\rho_1^{b,A} + \rho_2^{b,A}) - (\rho_1^{b,B} + \rho_2^{b,B})}, \quad i = 1,2. \tag{26}$$

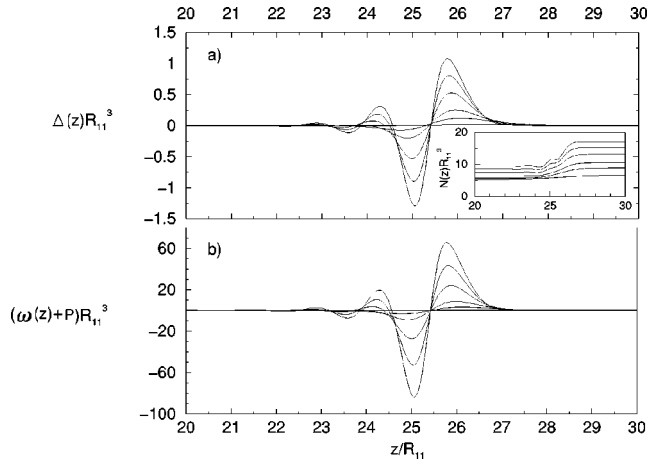

FIG. 11. The top graph (a) shows the function $\Delta(z)$ obtained from the density profiles shown in Figs. 6 and 7. $\Delta(z)$, defined by Eq. (25), measures the surface segregation at the interface. Below it in (b) is plotted $[\omega(z) + P]$, the integral of which is the surface tension. Each set of curves corresponds to state points A–F on the phase diagram (Fig. 1); the most oscillatory refers to state F. Apart from the scales on the y axes the two sets of curves are almost identical, demonstrating that the surface tension arises primarily from concentration fluctuations. The total density $N(z) = \rho_1(z) + \rho_2(z)$, shown in the inset to (a), has very different variation from the surface tension integrand.

with A and B referring to the two coexisting phases. Clearly $a_1 + a_2 = 1$. $\Delta(z)$ may also be expressed as

$$\Delta(z) = \frac{a_2[\rho_1(z) - \rho_1^{b,B}] - a_1[\rho_2(z) - \rho_2^{b,B}]}{a_1 a_2}. \tag{27}$$

The integral of $\Delta(z)$ yields the thermodynamic function $\Gamma_{2,1}$, i.e., the relative adsorption of species 2 with respect to species 1 [14]:

$$\Gamma_{2,1} = -a_2 \int_{-\infty}^{\infty} dz \Delta(z). \tag{28}$$

Thus $\Delta(z)$, which has the dimension of number density, measures the variation of local concentration through the interface. Figure 11 shows a plot of $\Delta(z)$ calculated from the profiles in Figs. 6 and 7. Below it is displayed $[\omega(z) + P]$, the integrand of Eq. (22), which gives the surface tension. Both functions are nonzero only in the interfacial region. The similarity between the two sets of curves shows that the major contribution to the surface tension comes from concentration fluctuations at the interface rather than from fluctuations of the total density since $N(z)$ has a very different form—see the inset to part (a) of the figure.

The situation is quite different for the perfectly symmetric mixture considered in Fig. 5. Because of the symmetry exhibited by the density profiles, $a_2\Delta(z) = \rho^b - N(z)$, where $\rho^b = \rho_1^{b,A} + \rho_2^{b,A}$ is the total density in both bulk phases. In Fig. 12 we compare plots of the surface tension integrand $[\omega(z) + P]$ and the function $\tilde{N}(z) \equiv \rho^b - N(z)$ corresponding

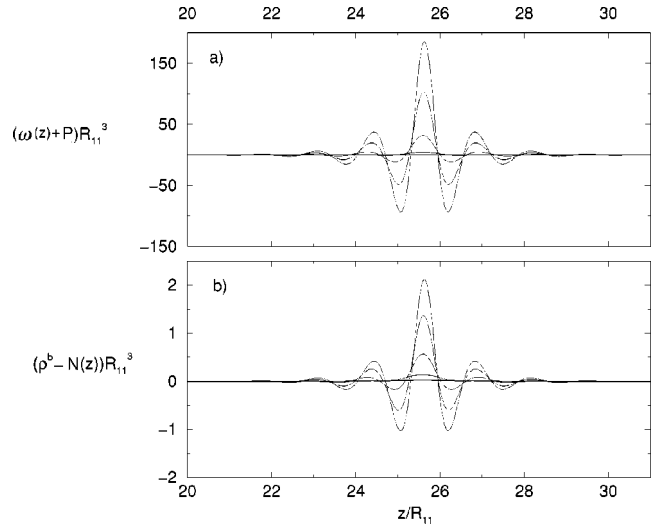

FIG. 12. The top graph (a) shows the function $[\omega(z)+P]$ obtained from the density profiles of the symmetrical mixture shown in Fig. 8, the integral of which is the surface tension. Below it in (b) is plotted the total density fluctuation variable $\tilde{N}(z)\equiv\rho^b - N(z)$. Apart from the scales on the *y* axes the two sets of curves are almost identical, demonstrating that the surface tension arises primarily from total density fluctuations.

to the density profiles of Fig. 8. It is clear that the two sets of curves are very similar.

IV. ASYMPTOTIC DECAY OF CORRELATION FUNCTIONS AND THE FISHER-WIDOM LINE

In this section we describe the asymptotic decay, $r\to\infty$, of the total pairwise correlation functions $h_{ij}(r)$ in our model mixture and the determination of the FW line. The basic procedure follows that in [12]. In Fourier space the Ornstein-Zernike equations for $h_{ij}(r)$ in terms of the pairwise direct correlation functions $c_{ij}(r)$ of a two-component liquid are

$$\hat{h}_{ij}(q)=\frac{N_{ij}(q)}{D(q)} \tag{29}$$

where $\hat{h}_{ij}(q)$ is the three-dimensional Fourier transform of $h_{ij}(r)$. The numerator is given by

$$N_{11}(q)=\hat{c}_{11}(q)+\rho_2^b(\hat{c}_{12}^2(q)-\hat{c}_{11}(q)\hat{c}_{22}(q)),$$

$$N_{22}(q)=\hat{c}_{22}(q)+\rho_1^b(\hat{c}_{12}^2(q)-\hat{c}_{11}(q)\hat{c}_{22}(q)),$$

$$N_{12}(q)=\hat{c}_{12}(q), \tag{30}$$

and

$$D(q)=[1-\rho_1^b\hat{c}_{11}(q)][1-\rho_2^b\hat{c}_{22}(q)]-\rho_1^b\rho_2^b\hat{c}_{12}^2(q). \tag{31}$$

Inverting the FT and noting that $\hat{h}_{ij}(q)$ is even we can write

$$rh_{ij}(r)=\frac{1}{4\pi^2 i}\int_{-\infty}^{\infty}dqqe^{iqr}\hat{h}_{ij}(q)$$

$$=\frac{1}{4\pi^2 i}\int_{-\infty}^{\infty}dqqe^{iqr}\frac{N_{ij}(q)}{D(q)} \tag{32}$$

which can be evaluated by contour integration [12]. From Eq. (5) it follows that within our mean-field treatment of the GCM

$$\hat{c}_{ij}(q)=-\beta\hat{v}_{ij}(q)=-\beta\pi^{3/2}R_{ij}^3\epsilon_{ij}\exp(-R_{ij}^2q^2/4) \tag{33}$$

and the singularities of $\hat{h}_{ij}(q)$ are simple poles. Choosing an infinite radius semicircle in the upper half of the complex plane, we obtain

$$rh_{ij}(r)=\frac{1}{2\pi}\sum_n e^{iq_nr}R_n^{ij} \tag{34}$$

where R_n^{ij} is the residue of $qN_{ij}(q)/D(q)$ for the nth pole at $q=q_n$. The q_n are solutions of $D(q_n)=0$ and there is normally an infinite number of poles. If a pole lies on the imaginary axis, $q_n=i\alpha_0$, it contributes a pure exponential term of the form $\exp(-\alpha_0 r)$ to the sum in Eq. (34). Poles lying off the imaginary axis occur in conjugate pairs $q_n=\pm\alpha_1+i\tilde{\alpha}_0$ and such a pair contributes a damped oscillatory term of the form $\exp(-\tilde{\alpha}_0 r)\cos(\alpha_1 r-\theta)$ to the sum in Eq. (34). The longest-range decay of $h_{ij}(r)$ is determined by the pole or the conjugate pair of poles with the smallest imaginary part. If $\alpha_0<\tilde{\alpha}_0$ the longest-range decay is monotonic (pure exponential), otherwise it is damped oscillatory. Since all three $\hat{h}_{ij}(q)$ have a common denominator $D(q)$ all three $h_{ij}(r)$ decay ultimately with the same decay length and wavelength; only the residues depend on the particular species and these determine only the amplitudes and phases of the leading order decay [12,15]. Similar arguments [12] apply for the one-body density profiles in a binary mixture and give rise to Eqs. (20) and (21). The α_0, $\tilde{\alpha}_0$, and α_1 appearing in these equations are determined by the poles of $\hat{h}_{ij}(q)$—as described above.

The FW line alluded to earlier is the crossover line in the phase diagram where $\alpha_0=\tilde{\alpha}_0$. As the fluid-fluid spinodal corresponds to points in the phase diagram at which the pure imaginary pole vanishes, i.e., $\alpha_0=0$, crossover from oscillatory to monotonic decay must occur before the spinodal is reached, which implies that the FW line lies below the spinodal in the (ρ,x) plane. By calculating the zeros of $D(q)$, i.e., the first few poles, for a range of state points it is straightforward to map out the FW lines displayed in Figs. 1–5.

For the first three cases, Figs. 1–3, the dashed FW line has two separate branches terminating in a cusp at low total density ρ_{cu}. As the mixture is made more asymmetric, i.e., R_{22}/R_{11} decreases, the right hand branch lies closer to the axis $x=1$. On the left hand branch the crossover (at fixed $\rho>\rho_{cu}$) is from longest-range oscillatory decay with wave-

length $2\pi/\alpha_1 \approx 2R_{11}$ to monotonic decay, whereas on the right hand branch it is from monotonic to oscillatory with wavelength $\approx 2R_{22}$. For $\rho < \rho_{cu}$ there is a separate crossover line, denoted by the solid line in the bottom right corner of Figs. 1–3. On each side the long-range decay is given by

$$rh_{ij}(r) \sim \tilde{A}_{ij} \exp(-\tilde{\alpha}_0 r)\cos(\alpha_1 r - \theta_{ij}) + \tilde{\tilde{A}}_{ij} \exp(-\tilde{\tilde{\alpha}}_0 r)\cos(\alpha_1' r - \theta_{ij}'), \quad r \to \infty, \tag{35}$$

where $\alpha_1 \approx \pi/R_{11}$ and $\alpha_1' \approx \pi/R_{22}$. To the left of the line $\tilde{\alpha}_0 < \tilde{\tilde{\alpha}}_0$ while on the right, $\tilde{\alpha}_0 > \tilde{\tilde{\alpha}}_0$, i.e., there is crossover from oscillatory decay with one wavelength to oscillatory decay with another wavelength when $\tilde{\alpha}_0 = \tilde{\tilde{\alpha}}_0$. At the cusp, where the two branches of the FW line meet this line, the pure imaginary (monotonic) pole $\alpha_0 = \tilde{\alpha}_0 = \tilde{\tilde{\alpha}}_0$.

Making the mixture more symmetric shifts the cusp to smaller x and for $R_{22}/R_{11} > 0.707$ there is no cusp in the FW line and the crossover line separating regions with different types of oscillatory decay is absent—see Figs. 4 and 5. Further details of the pole structure that gives rise to the crossover lines will be given elsewhere.

To the best of our knowledge this is the first time that the FW line has been mapped out for a binary mixture exhibiting fluid-fluid phase separation of the type displayed here [16] and it is important to inquire how robust results based on the simple RPA (5) might be. For the pure GCM the comprehensive study of Louis *et al.* [8] showed that for $\epsilon^* = 2$ the radial distribution functions $g(r)$ obtained from the hypernetted chain approximation were virtually indistinguishable from Monte Carlo data at reduced densities $\rho R^3 = 0.1$, 0.5, and 2.0. These authors also argued that the HNC should become exact in the high density limit and suggested that the HNC pair correlation function should provide an (''exact'') reference against which other approximations might be gauged. In this spirit we compare, in Fig. 13, the RPA results for $g(r)$ with those obtained from our own HNC calculations at reduced densities ρR^3 2, 4, and 6. As the density is increased the correlation hole is reduced and the degree of particle overlap increases, leading to a $g(r)$ that is closer to that of the ideal gas [8]. For $\rho R^3 = 2$ the RPA result lies well below the HNC for $r/R \lesssim 0.4$, i.e., in the central overlap region. However, for $\rho R^3 = 6$ the two closures yield very similar results for all except the smallest separations r. What is more significant for our present purposes is that for all three densities the simple RPA result is very close to that of the HNC for *large* separations, i.e., $r/R \gtrsim 0.8$. In particular, the oscillations in $g(r)$ are very well captured by the RPA—see the inset to Fig. 13. This implies that the RPA provides a rather accurate account of the asymptotic decay of $g(r)$ and therefore of the leading pole in $\hat{h}(q)$ [17], at least for reduced densities $\gtrsim 2$. But this is the range of (total) densities most relevant in determining the FW lines in the mixtures (see Figs. 1–5) so we are confident that our results for the latter should be qualitatively correct.

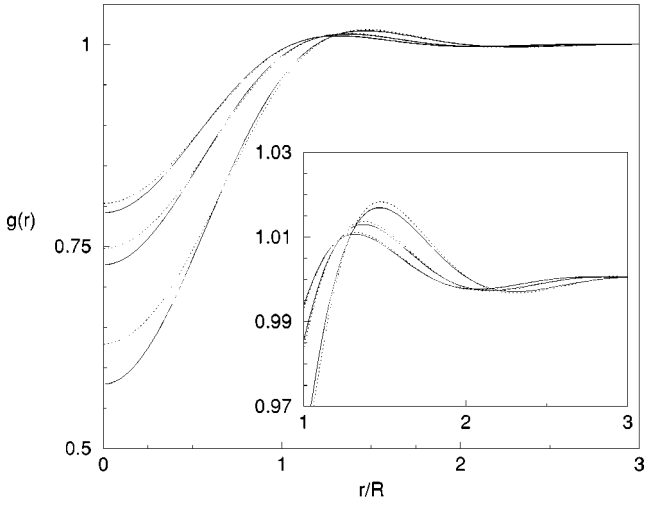

FIG. 13. The radial distribution function $g(r)$ for a pure fluid of Gaussian particles with $\epsilon^* = 2$ and radius R, calculated at reduced densities $\rho R^3 = 2,4,6$ (from bottom to top). For each density the dotted line is the HNC result and the solid line is that of the RPA closure. The inset shows a magnification of the oscillations.

Further evidence for the existence of the oscillatory-oscillatory crossover line comes from considering the low density approximation

$$c_{ij}(r) = f_{ij}(r) \equiv \exp[-\beta v_{ij}(r)] - 1 \tag{36}$$

where $f_{ij}(r)$ denotes the Mayer function. We calculated the zeros of $D(q)$, Eq. (31), using this approximation and found a crossover line approaching $\rho = 0$, $x = 1$, similar to that shown in the bottom right corner of Figs. 1 and 2.

Finally, we should remark that the accuracy of the RPA for determining the spinodal and the fluid-fluid coexistence curve of the binary GCM has been examined by Finken *et al.* [18]. For parameters close to those employed in Fig. 1 They find that the HNC and the RPA coexistence curves are close.

V. DISCUSSION

In this paper we have calculated the properties of the planar interface between two coexisting fluid phases in the binary GCM using the simplest mean-field free energy functional (3). We considered various choices of the size ratio R_{22}/R_{11}, employing the rule (12) for the range parameter R_{12}. It is the positive nonadditivity embodied in Eq. (12) that drives the demixing in Figs. 2–4 since the corresponding energy parameters favor mixing, i.e., $\epsilon_{11}^* = \epsilon_{22}^* \geqslant \epsilon_{12}^*$. The surface tension in these systems is governed by the segregation $\Delta(z)$, which measures the local relative concentration in the interface, rather than by the local total density $N(z)$—see Fig. 11. For comparison we also considered a symmetric system with $R_{22}/R_{11} = 1.0$ and $\epsilon_{12}^* > \epsilon_{11}^*$ where the demixing is driven by energy considerations. Symmetry then dictates that the phase diagram is symmetric about $x = 0.5$ (Fig. 5) and the surface tension is governed by $N(z)$—see Fig. 12. However, in all the cases we considered, plots of the reduced surface tension γ^* versus the order parameter $(\rho_1^{b,A}$

$-\rho_1^{b,B})R_{11}^3$ showed similar behavior to those in Figs. 9 and 10 with γ^* vanishing at the critical point as $(\rho_1^{b,A}-\rho_1^{b,B})^3$. Beyond the mean field approximation to the exponent should be replaced by the ratio $2\nu/\beta$, where ν denotes the correlation length and β the coexistence curve (order parameter) critical exponent, respectively. As we expect the critical behavior of this system to lie in the Ising universality class, for which $2\nu/\beta \sim 3.9$, the curves in Figs. 9 and 10 should, in reality, be flatter near the origin.

The most striking aspect of our results (Figs. 6 and 8) is the presence of pronounced oscillations in the interfacial density profiles for certain thermodynamic states. We accounted for the occurrence of damped oscillations in terms of general arguments involving the asymptotic decay of the bulk pairwise correlation functions $h_{ij}(r)$, i.e., by means of an analysis of the leading poles of $\hat{h}_{ij}(q)$ and determination of the FW lines that parallels earlier DFT treatments of interfaces [9,10]. The oscillations arise from packing effects which are still present in these soft-core systems. Although our present mean-field functional (2) should provide reliable estimates for $\tilde{\alpha}_0$ and α_1 and hence for the decay length and wavelength of the oscillations [see Eq. (21)], it is not clear that it will yield reliable amplitudes $\tilde{A}_i$. The latter depend on the strength and extent of the inhomogeneity rather than on properties of the bulk phase. Thus for states such as *E* and *F* in Fig. 1, which are very far from the critical point and deep in the oscillatory region of the phase diagram, the theory must treat density profiles that decrease from $\rho_1 R_{11}^3 \simeq 9$ to extremely low values $\rho_1 R_{11}^3 \simeq 0.03$ over a distance of about $2R_{11}$ (see Fig. 6). One would certainly expect the functional (i.e., the RPA) to fail in the very low density region. The situation seems rather more favorable for species 2 (Fig. 7) where $\rho_2 R_{11}^3 \geqslant 0.3$ throughout the interface for all states. However, even for state *F*, the oscillations in $\rho_2(z)$ are extremely weak! The total density $N(z)$ is, of course, large throughout the interface and shows only mild variation for all states (see the inset to Fig. 11). But the theory must be able to describe the individual profiles. These exhibit a degree of inhomogeneity that is higher than for the pure GCM near a hard wall where the functional performs well [8]. We believe that a more refined DFT, which incorporates a more accurate treatment of low densities, might yield smaller amplitudes for the oscillations in $\rho_1(z)$ without significantly altering their decay length and wavelength [19].

All approximate DFT treatments omit the effects of capillary-wave fluctuations of the interface [20]. Incorporating the latter usually requires some *ad hoc* prescription. The standard procedure is to assume that DFT furnishes the ''bare'' or ''intrinsic'' profiles—which might be oscillatory, as in the present case—and that fluctuations can be unfrozen on these. At the simplest level one performs a Gaussian smearing of the profiles over the interfacial thermal roughness $\xi_\perp$. If the profile has an oscillatory tail with the form of Eq. (21) one finds that the wavelength $2\pi/\alpha_1$ and decay length $\tilde{\alpha}_0^{-1}$ are unaltered but the amplitude is reduced by a factor $\exp[-(\alpha_1^2-\tilde{\alpha}_0^2)\xi_\perp^2/2]$ [12,21]. As we have seen, α_1 is an intrinsic property of the bulk fluid and is approximately π/R_{11} or π/R_{22}. The roughness $\xi_\perp$ depends on the interfacial area L_x^2 and on the external potential, e.g., gravity, that might be present at a real planar interface. If we ignore the latter $\xi_\perp^2 = (2\pi\beta\gamma)^{-1}\ln(K_{max}/K_{min})$ where K_{max} and K_{min} are the upper and lower cutoff wave numbers for the capillary-wave fluctuations [20]. We may take $K_{min} = 2\pi/L_x$ and $K_{max} = 2\pi/\xi$ where $\xi \equiv \tilde{\alpha}_0^{-1}$ is the bulk correlation length. It follows that the amplitude of the oscillations in the density profile should be reduced by a factor $(L_x/\xi)^{-\omega[(\alpha_1/\tilde{\alpha}_0)^2-1]}$ where $\omega \equiv (4\pi\beta\gamma\xi^2)^{-1}$ is the standard dimensionless parameter that measures the strength of capillary-wave fluctuations. Clearly, the larger the value of ω, i.e., the smaller the surface tension γ, the more damped are the oscillations. What is significant about this formula is that the amplitude is predicted to have a power-law dependence on the interfacial area L_x^2. This prediction has been examined by Toxvaerd and Stecki [22] in molecular dynamics simulations of a liquid-liquid interface. Their model is an equimolar binary mixture in which the 11 and 22 interatomic potentials are identical [both are (truncated) Lennard-Jones], whereas the 12 potential is purely repulsive. Thus their model mixture resembles the symmetric case in our present study. For small L_x the density profiles reported in [22] exhibit oscillations similar to those in Fig. 8. The oscillations appear to be insensitive to the length of the simulation box (perpendicular to the interface) but their amplitude depends on the area L_x^2 of the box. Increasing L_x reduces the amplitude in a manner that is consistent with power-law decay [22], lending support to the picture of ''Gaussian unfreezing'' of fluctuations on an intrinsic profile that is oscillatory.

It is important to consider the various length scales in the problem. For the mixture in Ref. [22] we expect $\xi \sim \sigma$, the Lennard-Jones diameter, and $\alpha_1 \sim 2\pi/\sigma$ for states well removed from the critical point where pronounced oscillations are observed. σ would be a few angstroms if we were modeling an atomic mixture. In our present GCM we have in mind polymers where the radius of gyration R_{11} is, of course, much longer. Nevertheless, it is evident that the absolute length scales cancel out in the combinations $(\alpha_1/\tilde{\alpha}_0)^2-1$ and ω. Thus one might expect similar power laws for the damping of oscillations with interfacial area. Detailed estimates depend on the precise values of the reduced tension γ^*, $\tilde{\alpha}_0$, and α_1. As an illustration we consider the symmetric case of the GCM with total bulk density $\rho R_{11}^3 = 14$ where the oscillations are fairly well pronounced—see Fig. 8. At coexistence we find $\alpha_1 R_{11} = 4.69$, $\tilde{\alpha}_0 R_{11} = 1.34$, and the reduced surface tension $\gamma^* = 17.1$, which implies $\omega = 8.37\times 10^{-3}$ and $(\alpha_1/\tilde{\alpha}_0)^2 - 1 = 11.3$. Thus the exponent in the power-law is -0.1, implying that the amplitude of the oscillations is only weakly damped by the capillary-wave fluctuations. If we repeat the calculation for the interface simulated by Toxvaerd and Stecki [22], using their values $\tilde{\alpha}_0\sigma = 0.28$, $\alpha_1\sigma = 6.98$, and $\gamma^* \equiv \beta\gamma\sigma^2 = 2.7$, we find a much stronger damping: the exponent is -1.4. For the liquid-vapor interface of a simple one-component fluid near its triple point the corresponding exponent is usually estimated to be about -3. In other words, our present binary GCM exhibits a particularly

''stiff'' interface for those states where the oscillations in the mean-field treatment are pronounced. Of course, these states are far from the critical point and correspond to very high total densities and very high surface tensions. One does not observe such a situation at the liquid-vapor interface of the one-component fluid since the triple point (solid phase) intervenes. There should be no solid phases in the relevant high density region of the phase diagram of the binary GCM. This suggests that computer simulations of the fluid-fluid interface might be very revealing [23].

To conclude, we return to possible applications of the binary GCM to mixtures of polymers. As mentioned in the Introduction, the effective interaction between two identical isolated nonintersecting polymer chains, averaged over the internal conformations, is well represented by a Gaussian whose width R is of the same order as the radius of gyration and whose height is a few k_BT. Note that the effective potential is entropic, so that ϵ is simply proportional to the temperature T, for an athermal solvent [6]. Recently, Louis *et al.* [5] have shown that the Gaussian shape remains a good approximation to the effective potential in dilute and semidilute solutions of self-avoiding random walk (SAW) polymers and that the parameters ϵ and R do not vary strongly with the concentration of the polymer: $\epsilon \simeq 2k_BT$. The same authors showed that the Gaussian effective potential reproduces the structure and thermodynamic properties of SAW polymer solutions over a wide concentration range. Such a procedure has great appeal as the monomer degrees of freedom no longer appear; one treats the chains as ''soft colloids'' [5]. Much less is established for mixtures of polymers; it is not known how well the phase separation found for the GCM (using the RPA and the HNC [18]) accounts for that which is observed at high concentration in mixtures of polymers with different chain lengths [24]. Phase separation is, of course, also observed in polymer blends (melts). Given the predictions of rich interfacial behavior that have emerged from the present study of the GCM, it would be worthwhile to pursue further possible connections between demixing in polymer systems and in the GCM.

As a final remark we note that the binary Gaussian core model is very different from the binary Gaussian model introduced by Helfand and Stillinger [25]. In the latter $v_{11}(r) = v_{22}(r) = 0$ while the Mayer f function $f_{12}(r) \equiv \exp[-\beta v_{12}(r)] - 1$ is a Gaussian. This model also exhibits fluid-fluid phase separation at high densities [25].

ACKNOWLEDGMENTS

We benefited from helpful discussions with J. M. Brader, C. N. Likos, A. A. Louis, G. Kahl, and R. Roth. We are grateful to R. Finken and A. J. Masters for informing us of the results of their calculations. A.J.A. was supported by EPSRC.

[1] F. H. Stillinger, J. Chem. Phys. **65**, 3968 (1976).
[2] F. H. Stillinger and D. K. Stillinger, Physica A **244**, 358 (1997).
[3] A Gaussian effective potential for polymers was first proposed by P. J. Flory and W. Krigbaum, J. Chem. Phys. **18**, 1086 (1950).
[4] J. Dautenhahn and C. K. Hall, Macromolecules **27**, 5399 (1994), and references therein.
[5] A. A. Louis, P. G. Bolhuis, J-P. Hansen, and E. J. Meijer, Phys. Rev. Lett. **85**, 2522 (2000); P. G. Bolhuis, A. A. Louis, J-P. Hansen, and E. J. Meijer, J. Chem. Phys. **114**, 4296 (2001).
[6] For an illuminating survey, see C. N. Likos, Phys. Rep. **348**, 267 (2001).
[7] A. Lang, C. N. Likos, M. Watzlawek, and H. Löwen, J. Phys.: Condens. Matter **12**, 5087 (2000). By making comparison with simulations C. N. Likos, A. Lang, M. Watzlawek, and H. Löwen [Phys. Rev. E **63**, 031206 (2001)] have established the validity of the RPA at high densities for bounded, positive definite pair potentials in general.
[8] A. A. Louis, P. G. Bolhuis, and J-P. Hansen, Phys. Rev. E **62**, 7961 (2000).
[9] R. Evans, J. R. Henderson, D. C. Hoyle, A. O. Parry, and Z. A. Sabeur, Mol. Phys. **80**, 755 (1993).
[10] J. M. Brader, R. Evans, M. Schmidt, and H. Löwen (unpublished).
[11] M. E. Fisher and B. Widom, J. Chem. Phys. **50**, 3756 (1969).
[12] R. Evans, R. J. F. Leote de Carvalho, J. R. Henderson, and D. C. Hoyle, J. Chem. Phys. **100**, 591 (1994).
[13] J. M. Brader and R. Evans, Europhys. Lett. **49**, 678 (2000).
[14] M. M. Telo da Gama and R. Evans, Mol. Phys. **48**, 229 (1983).
[15] G. A. Martynov, *Fundamental Theory of Liquids: Methods of Distribution Functions* (Hilger, Bristol, 1992).
[16] Previous studies have focused on models such as the RPM (restricted primitive model) and the Yukawa-RPM, designed for ionic fluids—see R. J. F. Leote de Carvalho and R. Evans, Mol. Phys. **92**, 211 (1997), and references therein.
[17] It is possible to calculate the leading pole from numerical solutions of the HNC—see R. J. F. Leote de Carvalho, R. Evans, and Y. Rosenfeld, Phys. Rev. E **59**, 1435 (1999). The same study of the OCP (one-component plasma) showed that retaining only the leading pole contribution yields an excellent fit to $g(r)$ for r down to the position of the first maximum.
[18] R. Finken, A. A. Louis, and J.-P. Hansen (unpublished).
[19] A. J. Masters (private communication) has made such a modification and used this to investigate the interfacial profiles of a binary mixture of particles interacting via repulsive parabolic potentials. He finds the modification does reduce the amplitude of the oscillations.
[20] R. Evans, in *Fundamentals of Inhomogeneous Fluids*, edited by D. Henderson (Dekker, New York, 1992), Chap. 3, and references therein.
[21] L. V. Mikheev and A. A. Chernov, Zh. Eksp. Teor. Fiz. **92**, 1732 (1987) [Sov. Phys. JETP **65**, 971 (1987)].
[22] S. Toxvaerd and J. Stecki, J. Chem. Phys. **102**, 7163 (1995).
[23] We note that A. J. Masters and P. B. Warren (private communication) have performed dissipative particle dynamics simu-

lations of the model mentioned in Ref. [19]. They find oscillatory density profiles. An earlier simulation study [R. D. Groot and P. B. Warren, J. Chem. Phys. **107**, 4423 (1997)] describes the model and the technique and examines the validity of mean-field theory for the pure fluid and the mixture.

[24] In order to introduce phase separation, it may be necessary to introduce explicit monomer-monomer repulsion in the underlying polymer system [A. A. Louis (private communication)].

[25] E. Helfand and F. H. Stillinger, J. Chem. Phys. **49**, 1232 (1968). See also A. Baram, M. W. Maddox, and J. S. Rowlinson, Mol. Phys. **76**, 1093 (1992).